

Magnetic oscillations of critical current in intrinsic Josephson-junction stacks

A. E. Koshelev

Materials Science Division, Argonne National Laboratory, Argonne, Illinois 60439

(Dated: October 23, 2019)

A key phenomenon related to the Josephson effect is oscillations of different properties of superconducting tunneling junctions with magnetic field. We consider magnetic oscillations of the critical current in stacks of intrinsic Josephson junctions, which are realized in mesas fabricated from layered high-temperature superconductors. The oscillation behavior is very different from the case of a single junction. Depending on the stack lateral size, oscillations may have either the period of half flux quantum per junction (wide-stack regime) or one flux quantum per junction (narrow-stack regime). We study in detail the crossover between these two regimes. Typical size separating the regimes is proportional to magnetic field meaning that the crossover can be driven by the magnetic field. In the narrow-stack regime the lattice structure experiences periodic series of phase transitions between aligned rectangular configuration and triangular configuration. Triangular configurations in this regime are realized only in narrow regions near magnetic-field values corresponding to integer number of flux quanta per junction.

I. INTRODUCTION

Layered high-temperature superconducting materials, such as $\text{Bi}_2\text{Sr}_2\text{CaCu}_2\text{O}_x$ (BSCCO), are composed of superconducting cuprate layers coupled by Josephson interaction. This system possesses the Josephson effects at the atomic scale (“Intrinsic Josephson Effect”). A rich spectrum of classical *dc* and *ac* Josephson phenomena have been observed in this system, see reviews 1,2.

In a bulky superconductor the magnetic field applied along the layers generates a triangular lattice of Josephson vortices. The anisotropy factor γ and the inter-layer periodicity s set the important field scale, $B_{\text{cr}} = \Phi_0/(2\pi\gamma s^2)$ (~ 0.5 tesla for BSCCO). When the magnetic field exceeds B_{cr} the Josephson vortices homogeneously fill all layers.³ Strong coupling between the vortex arrays in neighboring layers mediated by the in-plane supercurrents⁴ determines the static and dynamic properties of the lattice. Dynamic properties of the Josephson-vortex lattice in BSCCO have been extensively studied by several experimental groups (see, e.g., Refs. 5,6,7,8).

When an external transport current flowing across the layers exceeds the *critical current*, the Josephson vortex lattice starts to move. In a homogeneous junction the critical current is determined by interaction with the boundaries. The simplest and most known case is a single small junction without inhomogeneities, where the field dependence of the critical current is given by the Fraunhofer dependence, $I_c(\Phi) = I_{c0}|\sin(\pi\Phi/\Phi_0)|/(\pi\Phi/\Phi_0)$, with Φ being the magnetic flux through the junction. Observation of this dependence has been considered as an important confirmation of the *dc* Josephson effect.⁹ The same dependence is also expected for the junction stack with the lateral size smaller than the Josephson length.¹⁰ In a single long junction the critical current has the rather complicated field dependence due to multiple coexistent states of the lattice.¹¹

In the previous paper 12 we considered the behavior of the critical current for the dense Josephson-vortex lat-

tice in a homogeneous wide stack for which the critical current is caused by interaction with the boundaries. We found that the boundary induces an alternating deformation of the lattice. Averaging out the rapid phase oscillations, we obtained that the lattice deformation obeys the sine-Gordon equation and decays inside superconductor at the typical length $L_B/\sqrt{8}$, which is larger than the Josephson length, $\lambda_J = \gamma s$, and increases proportional to the magnetic field, $L_B = \lambda_J B/B_{\text{cr}}$.¹³ The stack is in the wide-stack regime if its lateral width L is larger than this typical length. In this situation the surface deformation and the total current flowing along the surface is uniquely determined by the lattice position far away from the boundaries. The surface current has oscillating dependence on the lattice displacement and, due to the triangular-lattice ground state, the period of this dependence is half the lattice spacing. The total current flowing through the stack is given by the sum of two independent surface currents flowing at the sample edges. The magnetic field determines the magnitude of the maximum surface current (it is inversely proportional to the field) and sets the phase shift between the oscillating dependences of the two surface currents on the lattice position. One can trace that, due to the half-lattice-spacing periodicity of the surface current, a full period change of this phase shift corresponds to the change of the magnetic flux through one junction, Φ , equal to the half flux quantum, $\Phi_0/2$. As a consequence, the maximum current through the stack has oscillating field dependence, which resembles the Fraunhofer dependence: it has strong oscillations and overall $1/B$ dependence. However, the period of these oscillations is two times smaller: it corresponds to adding one flux quantum per two junctions and the critical current has local maxima at $\Phi = k\Phi_0/2$.

Oscillations of the flux-flow voltage in BSCCO mesas at slow lattice motion have been observed by Ooi *et al.*⁸ The oscillations have the period of $\Phi_0/2$ per junctions and are caused the size-matching effect described in the previous paragraph. These oscillations have been reproduced by numerical simulations.¹⁴ More recently the

flux-flow oscillations in BSCCO mesas have been reproduced and studied in more details by several experimental groups.^{15,16,17,18} Similar oscillations also have been observed in underdoped $\text{YBa}_2\text{Ca}_3\text{O}_{6+x}$.¹⁹ Size dependence of oscillations has been systematically studied in Refs. 15,17. It was found that at smaller lateral sizes and/or higher magnetic fields the crossover to the new oscillation regime takes place, in which the period becomes Φ_0 per junction, as in a single junction.

Being motivated by recent experiments, in this paper we extend our consideration to the regime when the junction size L is comparable with the length L_B and the system crosses over from the wide-stack to narrow-stack regime. As the length scale L_B increases with the magnetic field, it also sets the field scale $B_L = B_{cr}L/\lambda_J$, at which this length becomes of the order of the junction length L . Therefore for a junction of a given size the crossover to the narrow-stack regime can be driven by the magnetic field, as it was observed experimentally.¹⁵ $\Phi_0/2$ -periodicity of the critical-current oscillations holds until interactions between surface deformations can be neglected. This interaction becomes progressively stronger with decreasing the ratio L/L_B . Surface deformations at $L > L_B$ can be described as partial sine-Gordon solitons.²⁰ The relative sign of two solitons at the opposite edges is determined by the magnetic field and the lattice positions. At the integer-flux-quanta points $\Phi = k\Phi_0$ the surface solitons always have the same sign and repel each other. As a consequence, the amplitude of surface deformations drops and the critical current decreases. At the half-integer-flux-quanta points $\Phi = (k + 1/2)\Phi_0$ situation is the opposite: the surface solitons always have opposite signs and attract each other leading to enhancement of the surface deformations and increase of the critical current. Therefore the interaction between the surface solitons leads to the crossover between the $\Phi_0/2$ -periodic oscillations of the critical current and Φ_0 -periodic oscillations. This crossover occurs via suppression of the current peaks at the points $\Phi = k\Phi_0$ and enhancement of the current peaks at the points $\Phi = (k + 1/2)\Phi_0$. Such behavior is consistent with recent studies of the oscillations of the flux-flow voltage in mesas with small lateral sizes.^{15,16,17} The crossover in the voltage oscillations also has been studied numerically.^{16,21}

In the region $L \sim L_B$ the lattice structure is determined by competition between two energies: the interaction with boundaries and the bulk shearing interaction between the Josephson-vortex planar arrays in neighboring layers. The interaction with the boundaries favors the aligned rectangular arrangement of the Josephson vortices while the local shearing interaction favors the triangular lattice. The boundary interactions decay slower with increasing field than the shearing interaction and become dominating at large fields. On the other hand, the boundary interaction energy has oscillating field dependence and vanishes at the points $\Phi = k\Phi_0$. At these points the shearing interaction is relevant at any magnetic field. In addition, the interaction with the bound-

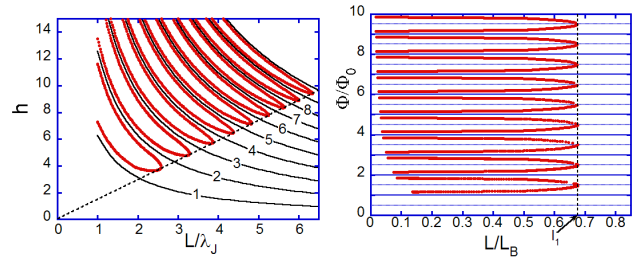


FIG. 1: *Left plot:* Phase diagram of the Josephson-junction stack in the coordinates [reduced junction size L/λ_J]-[reduced field $h = B/B_{cr}$]. The solid lines mark fields corresponding to the integer values of the magnetic flux per junctions, $\Phi = k\Phi_0$. Dotted lines show boundaries of the transitions into the rectangular lattice for ground state. *Right plot:* The same diagram in the coordinates [number of flux quanta per junction Φ/Φ_0]-[ratio $L/L_B \equiv L/(h\lambda_J)$].

aries is suppressed by the external current.

In the region $L \ll L_B$ the rectangular arrangement of vortices is realized in most part of the phase space and the field dependence of the critical current approaches the classical Fraunhofer dependence. Two important deviations persist at all fields and sizes: (i) Near the points $\Phi = k\Phi_0$ the phase transitions to the triangular lattice always take place. Critical current at these points never drops to zero and actually always has a small local maximum; (ii) Away from the points $\Phi = k\Phi_0$ the critical current is reached at the instability point of the rectangular vortex lattice and it is always somewhat smaller than the “Fraunhofer” value, $I_{c0}|\sin(\pi\Phi/\Phi_0)|/|\pi\Phi/\Phi_0|$. Therefore, we somewhat revise the statement of Ref. 10 that behavior of a small stack is identical to a single small junction. The described results has been summarized in a short paper published in the conference proceedings.²² The static lattice structures at different fields and sizes have been also studied numerically in Refs. 23 and 21 and the results are in a qualitative agreement with the described picture.

To illustrate a general picture, we show in Fig. 1 (left) the ground-state phase diagram of the junction stack in the field-size plane, where $h = B/B_{cr}$ is the reduced magnetic field. Solid lines mark the magnetic fields corresponding to integer values of the magnetic flux per junction and dotted lines show boundaries of the rectangular-lattice regions for zero current through the stack. As one can see, these regions appear above the line $h = 1.48L/\lambda_J$ and they are always bounded by the integer-flux quanta lines. In the right plot the same diagram is replotted in different coordinates, number of flux quanta per junction Φ/Φ_0 vs ratio $L/L_B \equiv L/(h\lambda_J)$, which controls the wide-stack/narrow-stack crossover. It is interesting to note that in these coordinates the diagram is periodic with respect to the magnetic flux through the junction.

The paper is organized as follows. In Section II we outline derivation of the phase distribution in the case

of alternating from layer to layer solution. Averaging with respect to the rapidly changing phase oscillations, we obtain equation and boundary conditions for the slow lattice deformation. We also express the lattice energy and current flowing through the stack via this deformation. In Section III we obtain and analyze solution for the smooth phase in terms of elliptic integrals. We found that the problem can be reduced to solution of three nonlinear coupled equations for three unknowns, the boundary phases and elliptic parameter. In Section IV we derive a criterion for the transition into the rectangular-lattice state. In Appendix B we consider weak finite-size effects in the wide-stack regime and analytically compute exponentially small finite-size corrections to the critical current, which break the $\Phi_0/2$ -periodicity of oscillations. In Section V we present results of numerical analysis of the crossover between the wide-stack and narrow-stack regimes with the increasing magnetic field. We obtain the oscillation patterns of the critical current for stacks with different lateral sizes and find location of the rectangular-lattice regions in the current-field plane. In Section VI we reanalyze in detail the narrow-stack regime using independent analytical approach. In Section VII we consider the voltage oscillations in the case of slowly moving lattice and relate these oscillations with the critical-current oscillations. We elaborate the recipe to extract the anisotropy factor from the voltage oscillations.

II. PHASE DISTRIBUTION AND ENERGY OF FINITE STACK ASSUMING ALTERNATING SOLUTION

We consider a Josephson-junction stack consisting of N layers, $N \gg 1$, with lateral size equal to L in a magnetic field $B > B_{cr}$ applied along the layers. At high magnetic fields one can neglect screening effects. In this case the stack is described by the energy functional (per layer and per unit length in the field direction) of the layer phases $\varphi_n(x)$,

$$E[\varphi_n] = \frac{1}{N} \sum_n \int_0^L dx \left[\frac{J}{2} \left(\frac{d\varphi_n}{dx} \right)^2 - E_J \cos \left(\varphi_{n+1} - \varphi_n - \frac{2\pi s B}{\Phi_0} x \right) \right]. \quad (1)$$

where J is the in-plane phase stiffness and E_J is the Josephson energy per unit area. To simplify derivations, we introduce reduced coordinate, $u = x/\lambda_J$, with $\lambda_J = \sqrt{J/E_J}$, reduced magnetic field, $h = 2\pi s \lambda_J B/\Phi_0$, and reduced energy $\mathcal{E} = E/(E_J \lambda_J)$. We also represent the phase variable in the form, which naturally describes the dense triangular lattice in the bulk in the limits $h \gg 1$ and $L/\lambda_J \gg h$, $\varphi_n(u) = \phi_n(u) + \alpha n + \pi n(n-1)/2$, where the phases $\phi_n(u)$ are assumed to be small and rapidly oscillating and the parameter α will describe lattice displacement. The the reduced energy per one junction and

per unit length in the field direction can now be represented as

$$\mathcal{E}[\phi_n] = \frac{1}{N} \sum_n \int_0^L du \left[\frac{1}{2} \left(\frac{d\phi_n}{du} \right)^2 - \cos(\phi_{n+1} - \phi_n - hu + \alpha + \pi n) \right]. \quad (2)$$

The oscillating behavior is determined by the reduced parameter hL which is directly related to the total magnetic flux through one junction $\Phi = BLs$,

$$hL = 2\pi\Phi/\Phi_0.$$

We consider the stack containing a very large number of junctions, $N \gg 1$. This will allow us to focus on bulk behavior and neglect c-axis boundary effects coming from the top and bottom junctions, which give $1/N$ corrections to the bulk results. We will also not consider potentially interesting ‘‘parity effects’’, small differences between stacks containing odd and even number of junctions, which have the same order. Our results are also not influenced by possible perturbations of the current distribution near the boundaries. Due to the large anisotropy of the material, the ‘‘bulk’’ current distribution usually is realized already in the second junction in the stack.

Following Ref. 12, we will assume the alternating phase distribution in the form $\phi_n = (-1)^n \phi$. This distribution describes both the deformed triangular lattice in the wide-stack regime and the transition to the rectangular lattice in narrow-stack regime. Substituting this presentation into Eq. (2), we represent the energy functional as

$$\mathcal{E}(\alpha; \phi) = \int_0^L du \left[\frac{1}{2} \left(\frac{d\phi}{du} \right)^2 - \sin(2\phi) \sin(-hu + \alpha) \right]. \quad (3)$$

The lattice energy as function of displacement, $\bar{\mathcal{E}}(\alpha)$, is determined by the minimum of the functional $\mathcal{E}(\alpha; \phi(u))$ with respect to $\phi(u)$, $\bar{\mathcal{E}}(\alpha) = \min_{\phi} [\mathcal{E}(\alpha; \phi)]$. As the energy functional has a symmetry property $\alpha \rightarrow \alpha + \pi$, $\phi \rightarrow -\phi$, the energy $\bar{\mathcal{E}}(\alpha)$ is π -periodic with respect to shift of α , $\bar{\mathcal{E}}(\alpha + \pi) = \bar{\mathcal{E}}(\alpha)$.

The ground-state phase distribution ϕ obeys the following equation

$$\frac{d^2\phi}{du^2} + 2 \cos(2\phi) \sin(-hu + \alpha) = 0, \quad (4)$$

which has to be solved with the boundary conditions

$$\frac{d\phi}{du} = 0, \text{ for } u = 0, L. \quad (5)$$

In the limit $h \gg 1$ further significant simplification is possible: we can average out rapid phase oscillations and derive a simplified equation for the smooth phase perturbation. We split the total phase into the smooth and rapidly-oscillating components

$$\phi(u) = v(u) + \tilde{\phi}(u), \quad (6)$$

where we assume $|\tilde{\phi}|, |dv/du| \ll 1$. The maximum value of $v(u)$, $v_{\max} = \pi/4$, corresponds to rectangular lattice. The rapidly-oscillating phase by definition obeys the equation

$$\frac{d^2\tilde{\phi}}{du^2} + 2\cos(2v)\sin(-hu + \alpha) = 0, \quad (7)$$

which has the following approximate solution

$$\tilde{\phi} \approx \frac{2}{h^2} \cos(2v)\sin(-hu + \alpha). \quad (8)$$

To the first order with respect to $\tilde{\phi}$, equation for $v(u)$ is given by

$$\frac{d^2v}{du^2} - 4\tilde{\phi}\sin(2v)\sin(-hu + \alpha) = 0.$$

Substituting into this equation the oscillating phase (8) and averaging it with respect to rapid oscillations, we finally obtain the sine-Gordon equation for the smooth phase

$$\frac{d^2v}{du^2} - \frac{2}{h^2} \sin(4v) = 0. \quad (9)$$

Computing the derivatives of the rapid phase (8) at the edges, we also derive the boundary conditions for the smooth phase,

$$\frac{dv}{du}(0) = \frac{2}{h} \cos(2v_0)\cos(\alpha), \quad (10a)$$

$$\frac{dv}{du}(L) = \frac{2}{h} \cos(2v_L)\cos(-hL + \alpha) \quad (10b)$$

with $v_0 \equiv v(0)$ and $v_L \equiv v(L)$. The local current density, $j(u) = j_J \sin[\theta_{n,n+1}(u)]$ with j_J being the maximum Josephson current density, is determined by the gauge-invariant phase difference, $\theta_{n,n+1}(u) \equiv \phi_{n+1} - \phi_n - hu + \alpha + \pi n$, which is related to $v(u)$ as

$$\begin{aligned} \theta_{n,n+1} &\approx -hu + \alpha + \pi n - (-1)^n 2v \\ &\quad - \frac{4}{h^2} \cos(2v)\sin(-hu + \alpha + \pi n). \end{aligned} \quad (11)$$

Substituting the phase presentation (6) and (8) into the energy (3) and averaging with respect to the rapid oscillations, we derive the energy functional in terms of the smooth phase v ,

$$\begin{aligned} \mathcal{E}(\alpha; v) &\approx \frac{1}{h} [\sin(2v_0)\cos(\alpha) - \sin(2v_L)\cos(-hL + \alpha)] \\ &\quad + \int_0^L du \left[\frac{1}{2} \left(\frac{dv}{du} \right)^2 - \frac{1 + \cos 4v}{2h^2} \right]. \end{aligned} \quad (12)$$

To shorten notations, we omitted the arguments h and L in $\mathcal{E}(\alpha, h, L; v)$. Minimization of this energy functional with respect to $v(u)$ gives the energy as a function of the lattice shift α , $\mathcal{E}(\alpha)$. Minimum of this energy with respect to α gives the ground state for given h and

L . Higher-energy states at other values of α typically carry a finite current. The total Josephson current flowing through the stack is proportional to $d\bar{\mathcal{E}}/d\alpha$. Taking derivative of the functional (12) with respect to α , assuming that at every α it is minimized with respect to $v(u)$, we obtain

$$J(\alpha) = \frac{1}{h} [-\sin(2v_0)\sin\alpha + \sin(2v_L)\sin(-hL + \alpha)]. \quad (13)$$

The unit of current in this equation is $j_J \lambda_J w$ where j_J is the Josephson-current density and w is the junction size in the field direction. An important consequence of this equation is that nonzero current exists only if the surface deformations v_0 and v_L are finite. Further analysis is based on Eqs. (9), (10), (12), and (13).

III. SOLUTIONS FOR SMOOTH PHASE

A general solution of the sine-Gordon equation (9) can be found in terms of elliptic integrals. From the first integral of Eq. (9) we obtain

$$\frac{dv}{du} = \delta_d \sqrt{2} \frac{\sqrt{1/m - \cos^2(2v)}}{h} \quad (14)$$

with $\delta_d \equiv \text{sign}[dv/du] = \pm 1$ and m is the elliptic parameter which has to be found from the boundary conditions. From this equation we obtain implicit equation for deformation $v(u)$,

$$\int_{v_0}^v \frac{dv}{\sqrt{1/m - \cos^2(2v)}} = \delta_d \sqrt{2} u/h. \quad (15)$$

To rewrite this equation using standard elliptic integrals, we introduce a new variable φ ,

$$\varphi = \pi/2 + 2v. \quad (16)$$

This variable has its own physical meaning: it describes *the alternating deformation of the interlayer phase difference with respect to the rectangular-lattice state*. In particular, $\varphi = 0$ corresponds to the rectangular lattice. Using these variables, we can rewrite Eq. (15) as

$$\sqrt{m} [F(\varphi, m) - F(\varphi_0, m)] = \delta_d \sqrt{8} L/h \quad (17)$$

where

$$F(\varphi, m) \equiv \int_0^\varphi \frac{dx}{\sqrt{1 - m \sin^2 x}}$$

is the incomplete elliptic integral of the first kind.²⁴

In the limit of very large L the deformation v has to vanish far away from edges meaning that $m \rightarrow 1$. For finite-size junctions, depending on hL and α , the solution $v(u)$ can be either monotonic or nonmonotonic. For the nonmonotonic solution the derivative dv/du and the parameter δ_d change sign inside. The monotonic solution can either change sign ($v_0 v_L < 0$, $m < 1$) or not

($v_0 v_L > 0$). For large L the monotonic solution corresponds to the two surface partial solitons of the same sign and the nonmonotonic case corresponds to the surface solitons of opposite signs. A mathematical structure of solutions for these two cases is different and we will consider them separately.

First, we find some general relations between the boundary phases and the parameter m . From the boundary conditions (10a), (10b), and Eq. (14) we obtain equations

$$\delta_0 \sqrt{1/m - \cos^2(2v_0)} = \sqrt{2} \cos(2v_0) \cos(\alpha), \quad (18a)$$

$$\delta_L \sqrt{1/m - \cos^2(2v_L)} = \sqrt{2} \cos(2v_L) \cos(hL - \alpha) \quad (18b)$$

with $\delta_0 = \delta_d(0)$ and $\delta_L = \delta_d(L)$ (for monotonic solution $\delta_0 = \delta_L$ and for nonmonotonic solution $\delta_0 = -\delta_L$). As $|v_{0,L}| < \pi/4$, the inequality $\cos(2v_{0,L}) > 0$ always holds meaning that $\delta_0 = \text{sign}[\cos \alpha]$ and $\delta_L = \text{sign}[\cos(hL - \alpha)]$. From the conditions (18) we obtain the following results for the boundary deformations

$$\cos(2v_0) = \sqrt{\frac{1/m}{1 + 2 \cos^2(\alpha)}} \quad (19a)$$

$$\cos(2v_L) = \sqrt{\frac{1/m}{1 + 2 \cos^2(hL - \alpha)}} \quad (19b)$$

or, in terms of variable φ (16),

$$\sin \varphi_0 = \sqrt{\frac{1/m}{1 + 2 \cos^2(\alpha)}}, \quad (20a)$$

$$\sin \varphi_L = \sqrt{\frac{1/m}{1 + 2 \cos^2(hL - \alpha)}}. \quad (20b)$$

From these considerations one can conclude that the monotonic solution realizes for all α 's for $hL = 2k\pi$ (magnetic flux per junction equals to integer number of flux quanta, $\Phi = k\Phi_0$) and the nonmonotonic solution realizes for $hL = (2k+1)\pi$ (magnetic flux equals to half-integer number of flux quanta, $\Phi = (k+1/2)\Phi_0$). If the magnetic flux through one junction is not close to these special values then the solution changes from monotonic to nonmonotonic depending on the lattice phase shift α . Location of different types of solution depending on hL and α is illustrated in Fig. 2.

One can distinguish two important special cases corresponding to symmetric locations of the lattice with respect to the boundaries. The first case, $\alpha = hL/2 + \pi k$, $v_L = -v_0$, corresponds to the monotonic solution and the second case, $\alpha = hL/2 + \pi/2 + \pi k$, $v_L = v_0$, corresponds to the nonmonotonic solution. The energy always has extremums at these values of α . Moreover, a detailed study shows that the ground state is always realized at one of these values of α . At large L the system switches between these locations in the vicinity of the points $hL = (2k+1/2)\pi$, as it is illustrated in Fig. 2.

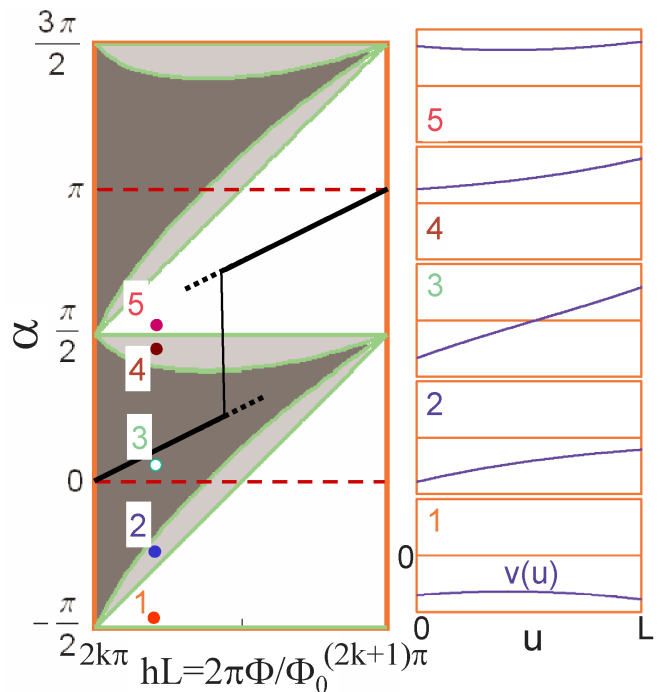


FIG. 2: Regions of different types of solution for the smooth alternating deformation $v(u)$ in the plane $hL-\alpha$ for $L/h \sim 1$. Typical solutions are illustrated for five marked points. Dark grey color marks regions of monotonic solution changing sign (3), light grey color marks regions of monotonic solution not changing sign (2 and 4), and white regions correspond to nonmonotonic solution (1 and 5). Light-grey regions shrink with increasing L . The black line illustrates the location of the ground state.

In the vicinity of these switching points the energy has minima at the both values of α .

In general, the conditions (19a) and (19b) are not sufficient to determine signs of the edge deformations v_0 and v_L . In the limit of large L the deformation $v(u)$ has to decay from the edges leading to relations $\text{sign}[v_0] = -\delta_0 = -\text{sign}[\cos \alpha]$ and $\text{sign}[v_L] = \delta_L = \text{sign}[\cos(hL - \alpha)]$. In this case we also obtain conditions

$$\tan(2v_0) = -\delta_0 \sqrt{m(2 \cos^2(\alpha) + 1) - 1},$$

$$\tan(2v_L) = \delta_L \sqrt{m(2 \cos^2(hL - \alpha) + 1) - 1}$$

which fix signs of v_0 and v_L . For large values of L/h monotonic solution typically changes sign inside. However for finite L there are intermediate regions exist located near lines $\alpha = \pi/2 + \pi k$ and $\alpha = hL + \pi/2 + \pi k$ where solution is still monotonic but does not change sign. We now proceed with analyzing separately the monotonic and nonmonotonic solutions.

A. Monotonic solution

The monotonic solutions realize for ranges of α where $\cos \alpha \cos(hL - \alpha) > 0$ (grey regions in Fig. 2). For such solution we obtain from Eq. (15) relation connecting the parameter m with the boundary deformations

$$\int_{v_0}^{v_L} \frac{dv}{\sqrt{1/m - \cos^2(2v)}} = \text{sign}[\cos \alpha] \sqrt{2L}/h. \quad (21)$$

Using previously introduced variable φ (16), we can rewrite Eq. (21) via elliptic integrals as

$$\sqrt{m} [F(\varphi_L, m) - F(\varphi_0, m)] = \text{sign}[\cos \alpha] \sqrt{8L}/h \quad (22)$$

This equation together with boundary conditions (20a), and (20b) have to be solved to find the three unknown constants φ_0 , φ_L , and m , which completely determine the solution. The boundary deformations $v_0 = (\varphi_0 - \pi/2)/2$ and $v_L = (\varphi_L - \pi/2)/2$ may have either the same sign or opposite signs. In Appendix A we find the boundary separating these two types of solution (boundaries between dark-grey regions and light-grey regions in Fig. 2).

The energy (12) and Josephson current (13) can be represented as

$$\begin{aligned} \mathcal{E} = & -\frac{1}{h} [\cos(\varphi_0) \cos(\alpha) - \cos(\varphi_L) \cos(hL - \alpha)] \\ & + \frac{1}{\sqrt{2mh}} |E(\varphi_L, m) - E(\varphi_0, m)| - \frac{L}{mh^2}, \end{aligned} \quad (23)$$

$$J(\alpha) = \frac{1}{h} [\cos(\varphi_0) \sin \alpha - \cos(\varphi_L) \sin(hL - \alpha)], \quad (24)$$

where $E(\varphi, m) \equiv \int_0^\varphi \sqrt{1 - m \sin^2 x} dx$ is the incomplete elliptic integral of the second kind.²⁴

B. Nonmonotonic solution

The solution is nonmonotonic in the regions given by $\cos \alpha \cos(hL - \alpha) < 0$ (white regions in Fig. 2). In this case the function $v(u)$ has extremum at some point $u = u_m$ so that we can rewrite Eq. (14) as

$$\begin{aligned} \frac{dv}{du} &= \delta_d \sqrt{2} \frac{\sqrt{1/m - \cos^2(2v)}}{h}, \quad \text{for } u < u_m, \\ \frac{dv}{du} &= -\delta_d \sqrt{2} \frac{\sqrt{1/m - \cos^2(2v)}}{h}, \quad \text{for } u_m < u < L \end{aligned}$$

with $\delta_d = \text{sign}[\cos \alpha]$. As $dv/du = 0$ at $u = u_m$, we have $m = 1/\cos^2(2v_m) > 1$ with $v_m \equiv v(u_m)$. Integrating the first equation from 0 to u_m and the second equation from L to u_m , we obtain

$$\begin{aligned} \int_{v_0}^{v_m} \frac{dv}{\sqrt{1/m - \cos^2(2v)}} &= \delta_d \sqrt{2} u_m / h, \\ \int_{v_L}^{v_m} \frac{dv}{\sqrt{1/m - \cos^2(2v)}} &= \delta_d \sqrt{2} (L - u_m) / h. \end{aligned}$$

Adding these two equations, we obtain equation connecting v_m with the boundary deformations v_0 and v_L

$$\begin{aligned} \int_{v_0}^{v_m} \frac{dv}{\sqrt{\cos^2(2v_m) - \cos^2(2v)}} \\ + \int_{v_L}^{v_m} \frac{dv}{\sqrt{\cos^2(2v_m) - \cos^2(2v)}} &= \delta_d \sqrt{2L}/h. \end{aligned} \quad (25)$$

This equation together with boundary conditions (19a) and (19b), represents the full system for determination of three unknown constants v_0 , v_L , and $m = 1/\cos^2(2v_m)$. To rewrite these equations in terms of elliptic functions, we again transfer to variable (16). Then equation (25) can be rewritten as

$$\sqrt{m} [2F(\varphi_m, m) - F(\varphi_0, m) - F(\varphi_L, m)] = \delta_d \frac{\sqrt{8L}}{h}. \quad (26)$$

with $\varphi_m = \pi/2 + 2v_m$. The boundary conditions in terms of φ_0 and φ_L are again given by Eqs. (20a) and (20b). The elliptic parameter is related to φ_m as $m = 1/\sin^2 \varphi_m$ leading to the following relation, $F(\varphi_m, m) = K(1/m)/\sqrt{m}$. The energy for nonmonotonic solution can be represented as

$$\begin{aligned} \mathcal{E} = & -\frac{1}{h} [\cos \varphi_0 \cos(\alpha) - \cos \varphi_L \cos(-hL + \alpha)] \\ & + \frac{1}{\sqrt{2mh}} |2E(\varphi_m, m) - E(\varphi_0, m) - E(\varphi_L, m)| - \frac{L}{mh^2} \end{aligned} \quad (27)$$

and the Josephson current is again given by Eq. (24). One can easily check that the nonmonotonic solution matches the monotonic solution at the boundaries. For example, for $\cos \alpha = 0$ the extremum is located at the boundary $u = 0$. In this case we have $\phi_0 = \phi_m = \arcsin(1/\sqrt{m})$ (or $\pi - \arcsin(1/\sqrt{m})$) and Eq. (26) coincides with Eq. (22).

C. Alternative presentation of equations via elliptic integrals

Using known relations for the elliptic integrals

$$\begin{aligned} F(\varphi, m) &= \frac{1}{\sqrt{m}} F(\psi, 1/m) \quad \text{with } \sin \psi = \sqrt{m} \sin \varphi, \quad (28a) \\ E(\varphi, m) &= \frac{1}{\sqrt{m}} [(1-m)F(\psi, 1/m) + mE(\psi, 1/m)], \end{aligned} \quad (28b)$$

valid for $\varphi < \pi/2$ and $\sin \varphi < 1/\sqrt{m}$, one can rewrite equations (22) and (20) for the case of the same-sign monotonic solution in the following alternative form

$$F(\psi_L, \tilde{m}) - F(\psi_0, \tilde{m}) = \text{sign}[\cos \alpha] \sqrt{8L}/h, \quad (29a)$$

$$\sin \psi_0 = \frac{1}{\sqrt{1 + 2 \cos^2(\alpha)}}, \quad (29b)$$

$$\sin \psi_L = \frac{1}{\sqrt{1 + 2 \cos^2(hL - \alpha)}}, \quad (29c)$$

with $\tilde{m} \equiv 1/m$. Correspondingly, the energy (23) in this representation is given by

$$\mathcal{E} = -\frac{1}{h} \left| \sqrt{1 - \tilde{m} \sin^2 \psi_0} \cos \alpha - \sqrt{1 - \tilde{m} \sin^2 \psi_L} \cos(hL - \alpha) \right| + \frac{1}{\sqrt{2}h} |E(\psi_0, \tilde{m}) - E(\psi_L, \tilde{m})| - \frac{(2 - \tilde{m})L}{h^2}. \quad (30)$$

In the case of nonmonotonic solution, using relations (28a) and (28b) for the elliptic integrals, one can rewrite equation (26) in the following equivalent form

$$2K(\tilde{m}) - F(\psi_0, \tilde{m}) - F(\psi_L, \tilde{m}) = \delta_d \sqrt{8}L/h. \quad (31)$$

where $\tilde{m} \equiv 1/m$, ψ_0 and ψ_L are given by Eqs. (29b) and (29c), and represent the energy as

$$\mathcal{E} = -\frac{1}{h} \left[\sqrt{1 - \tilde{m} \sin^2 \psi_0} |\cos \alpha| + \sqrt{1 - \tilde{m} \sin^2 \psi_L} |\cos(hL - \alpha)| \right] + \frac{1}{\sqrt{2}h} |2E(\tilde{m}) - E(\psi_0, \tilde{m}) - E(\psi_L, \tilde{m})| - \frac{(2 - \tilde{m})L}{h^2}. \quad (32)$$

This representation is especially useful in the case of large m (small \tilde{m}). In particular, it will allow us to study transition to the rectangular-lattice state corresponding to the limit $m \rightarrow \infty$, which we will consider in the next section.

IV. TRANSITION TO THE RECTANGULAR LATTICE

An important particular case is the solution of Eq. (9) corresponding to rectangular lattice, $v = \pm\pi/4$ or $\varphi = 0, \pi$. This case corresponds to the limit $m \rightarrow \infty$ ($\tilde{m} \rightarrow 0$). The energy of the rectangular lattice coincides with the well-known result for a single junction

$$\mathcal{E}_{\text{rect}}(\alpha) = -\frac{2}{h} \sin\left(\frac{hL}{2}\right) \sin\left(\alpha - \frac{hL}{2}\right) \quad (33)$$

and has minimum $\mathcal{E}_{\text{rect}} = -2|\sin(hL/2)|/h$ at $\alpha = hL/2 + \delta\pi/2$ with $\delta = \text{sign}[\sin(hL/2)]$.

To find condition for the transition to the rectangular lattice, we take the limit $\tilde{m} \rightarrow 0$ in Eq. (31) for nonmonotonic solution. Using relations $K(0) = \pi/2$ and $F(\psi, 0) = \psi$, we obtain

$$\pi - \psi_0 - \psi_L = \sqrt{8}L/h, \quad (34)$$

where ψ_0 and ψ_L are given by Eqs. (29b) and (29c). Using these definitions, the condition for the rectangular lattice can be rewritten in an explicit form as

$$\frac{\sqrt{2}(|\cos(hL - \alpha)| + |\cos \alpha|)}{\sqrt{(1 + 2\cos^2 \alpha)(1 + 2\cos^2(hL - \alpha))}} < \sin\left(\frac{\sqrt{8}L}{h}\right). \quad (35)$$

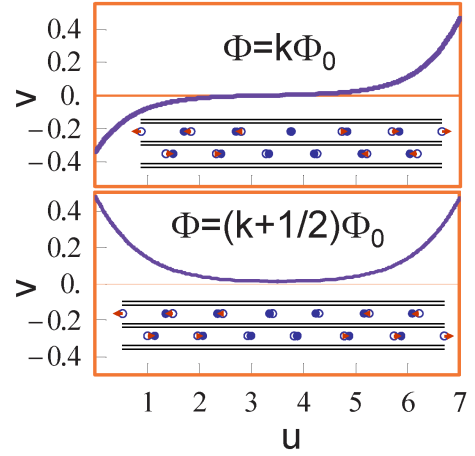


FIG. 3: Typical lattice deformations at large L for $\Phi = k\Phi_0$ (upper plot) and $\Phi = (k + 1/2)\Phi_0$ (lower plot). In the former case the surface partial solitons have the same sign and repel each other while in the latter case they have the opposite signs and attract each other. The insets in both plots illustrate corresponding displacement fields of the Josephson-vortex lattice in the two neighboring layers.

This equation gives the transition criterion in general case, including the current-carrying states. In particular, the rectangular lattice gives a local energy minimum at $\alpha = hL/2 + \pi/2$ in the regions $|hL/2\pi - (k + 1/2)| < 1/4$ if the inequality

$$|\sin(hL/2)| < \tan\left(\frac{\sqrt{2}L}{h}\right)/\sqrt{2} \quad (36)$$

is satisfied. The rectangular lattice first appears in the ground state at points $hL = (k + 1/2)2\pi$ for $L/h \leq l_1 = \arctan(\sqrt{2})/\sqrt{2} \approx 0.675$. This value is marked in the right plot of Fig. 1.

V. WIDE-STACK/NARROW-STACK CROSSOVER

In this section we investigate in detail the crossover between the wide-stack and narrow-stack regimes. As this crossover is driven by the reduced parameter h/L , for a junction with size L the crossover takes place with increasing magnetic field at size-dependent field $B_L = L\Phi_0/(2\pi\gamma^2 s^3)$.

At large L , $L \gg h$ or $B \ll B_L$, the smooth alternating deformation has solutions in the form of two isolated surface solitons.²⁰ The monotonic solution corresponds to the solitons of the same sign and the nonmonotonic solution corresponds to the solitons of opposite signs, as it is illustrated in Fig. 3. If one neglects the interaction between the solitons then the relative sign of surface soliton has no importance and the total Josephson current is given by the sum of two independent surface currents, which do not depend on the soliton signs.¹² As a con-

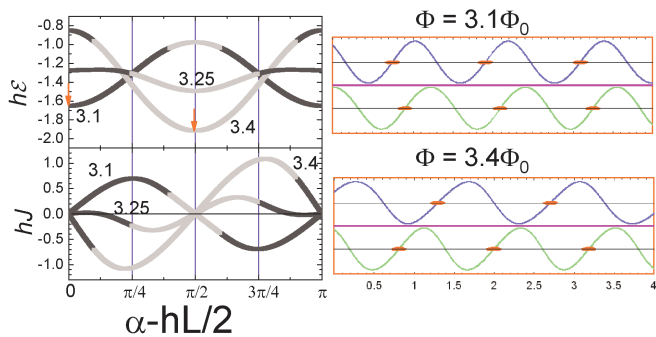


FIG. 4: The representative dependences of the energy (upper left plot) and Josephson current (lower left plot) on parameter α for $L = 4$ and three values of flux per junction $\Phi/\Phi_0 = 3.1, 3.25,$ and 3.4 within one oscillation period (the curves are marked by these values) corresponding to the magnetic fields $h = 4.87, 5.105,$ and 5.34 . The parameters correspond to the crossover region $L/h \sim 1$. Dark grey marks region of monotonic solution and light grey marks region of nonmonotonic solution. Arrows in the energy plot mark values of α corresponding to ground state. Pictures in the right column illustrate structure of ground states at $\Phi/\Phi_0 = 3.1$ and 3.4 . The lines show oscillating z -axis currents in neighboring layers and ellipses mark centers of the Josephson vortices.

sequence, the product hJ_c has periodicity of half flux-quantum per junction and reaches maxima at $hL = \pi j$ ($\Phi = j\Phi_0/2$) with $hJ_c \approx 1.035$. At finite L the interaction between the surface solitons disturbs such periodicity. At large L one can derive analytically corrections to the infinite- L results, see Appendix B for details. In particular, near the maxima $hL = \pi j$ ($\Phi = j\Phi_0/2$), we find the finite-size correction,

$$\delta J_c(h, \pi j) \approx -1.544 \frac{(-1)^j}{h} \exp\left(-\frac{\sqrt{8}L}{h}\right), \quad (37)$$

As we can see, the finite-size effects increase the critical current maxima at $\Phi = (k+1/2)\Phi_0$ ($j = 2k+1$) and reduce the critical current maxima at $\Phi = k\Phi_0$ ($j = 2k$). In the wide-stack regime, however, these corrections are exponentially small, which explains nice $\Phi_0/2$ -periodic oscillation of the flux-flow voltage observed in this regime.^{8,15}

In the whole range of fields and sizes we explore the phase diagram numerically. To find the ground state and the critical current at given h and L , we study dependences of the lattice structure, energy, and Josephson current on the lattice phase shift α . First, we have to find the boundary deformations φ_0, φ_L and the elliptic parameter m using the boundary conditions (20) together with either Eq. (22) for $\cos \alpha \cos(hL - \alpha) > 0$ or Eq. (26) for $\cos \alpha \cos(hL - \alpha) < 0$. Using obtained values, we compute the energy from Eq. (23) or (27) and the current from Eq. (24). This procedure has been implemented in Mathematica. Figure 4 shows representative α -dependences of the energy and current for $L = 4$ and three values of flux per junction $\Phi/\Phi_0 = 3.1, 3.25,$ and

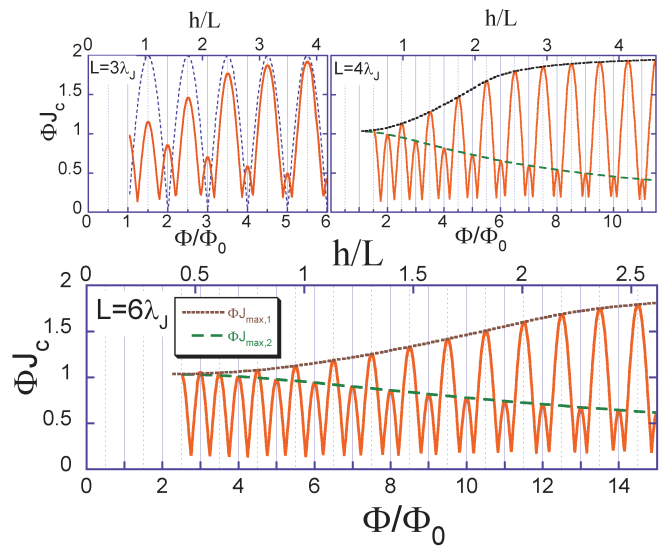


FIG. 5: The field dependences of the critical current for three different sizes $L = 3, 4,$ and 6 . To emphasize the periodic nature of dependences, we plot the product ΦJ_c (in units of $J_J \Phi_0 / 2\pi$ where J_J is the total maximum Josephson current) vs Φ/Φ_0 . One can observe the crossover from $\Phi_0/2$ -periodic oscillations to Φ_0 -periodic oscillations with increasing Φ . At larger L the crossover takes place at larger Φ/Φ_0 . The dashed line in the $L = 3\lambda_J$ plot shows function $2|\sin(\pi\Phi/\Phi_0)|$ corresponding to usual Fraunhofer dependence in small Josephson junctions. Top axes show the parameter h/L (in real units $h/L = B/B_L$ with $B_L = L\Phi_0/(2\pi\gamma^2 s^3)$). The crossover always takes place at the same value of ratio $h/L \sim 1.5$. In the plots for $L = 4\lambda_J$ and $6\lambda_J$ dotted and dashed lines show universal dependences of product Φ times current maxima at $\Phi = (k + 1/2)\Phi_0$ ($\Phi J_{max,1}$) and $\Phi = k\Phi_0$ ($\Phi J_{max,2}$) on the parameter h/L .

3.4 within one oscillation period. The minimum of the energy with respect to α determines the ground state and the maximum of the current determines the critical current.

Figure 5 shows the field dependences of the critical current for three different values of the junction size $L, 3, 4,$ and 6 . One can observe that with increasing field $\Phi_0/2$ -periodic oscillations smoothly transform into Φ_0 -periodic oscillations. This occurs via suppression of the peaks at $\Phi = k\Phi_0$ and enhancement of the peaks at $\Phi = (k + 1/2)\Phi_0$. Such behavior of the critical current has been recently reproduced by numerical simulations by Irie and Oya.²¹ Experimentally, the crossover between $\Phi_0/2$ - and Φ_0 -periodic oscillations has been observed in the flux-flow voltage by Kakeya *et al.*¹⁵ The crossover field can be arbitrarily defined as a field at which a $k\Phi_0$ -peak in the product ΦJ_c drops below the half of a $(k + 1/2)\Phi_0$ -peak. At larger L the crossover takes place at larger field and larger Φ/Φ_0 but it always occurs at the same ratio $h/L, h/L \sim 1.6$. Important property of the system, discussed in Sec. IV, is the transformation of the lattice into the rectangular state at sufficiently large h/L . This

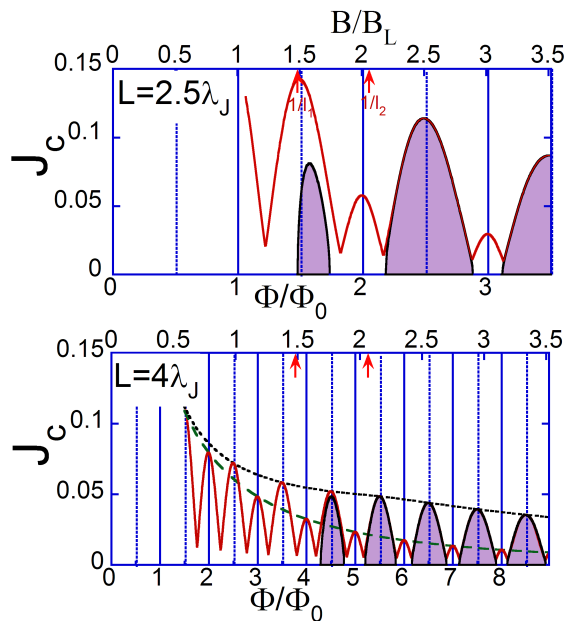


FIG. 6: The field dependences of the critical current (solid lines) for sizes $L = 2.5$, and 4 for the same range of the ratio h/L , $h/L \lesssim 3.5$ shown on the top axes. Shaded areas show the regions of stable rectangular lattice. The rectangular-lattice regions first appear in the vicinity of points $\Phi = (k + 1/2)\Phi_0$ when h/L exceeds $1/l_1 \approx 1.48$. When h/L exceeds $1/l_2 = 2.07$ the rectangular lattice remains stable at these points up to the critical current.

property is illustrated in Fig. 6 where behavior of the critical current is shown together with regions of stable rectangular lattice in the field-current diagram for two sizes, $L = 2.5$ and 4 .

Lets consider in more detail behavior of the critical-current maxima at $\Phi = (j/2)\Phi_0$. We start with the case of half-integer flux quanta per junction, $\Phi = (k + 1/2)\Phi_0$ ($hL = (2k + 1)\pi$). In this case a nonmonotonic solution is realized for all α . As for sufficiently high h/L the lattice transforms into rectangular state, it will be convenient to use presentation given by Eqs. (29b), (29c), and (31) which naturally describes this transition. As follows from Eq. (34), in the range

$$\cos \alpha > \tan(\sqrt{2}L/h)/\sqrt{2} \quad (38)$$

the rectangular lattice is realized for which $\tilde{m} = 0$ and the energy and current are given by

$$\begin{aligned} \mathcal{E}_1(\alpha) &= -\frac{2}{h} |\cos \alpha| \\ J_1(\alpha) &= \frac{2}{h} \sin \alpha \operatorname{sign}[\cos \alpha] \end{aligned}$$

In the opposite range, $\cos \alpha < \tan(\sqrt{2}L/h)/\sqrt{2}$, the solution has the form of deformed lattice. In this case we have $\psi_0 = \psi_L = \arcsin(1/\sqrt{1+2\cos^2 \alpha})$ (or

$\pi - \arcsin(1/\sqrt{1+2\cos^2 \alpha})$) and Eqs. (31) becomes

$$K(\tilde{m}) - F\left(\arcsin\left(\frac{1}{\sqrt{1+2\cos^2 \alpha}}\right), \tilde{m}\right) = \frac{\sqrt{2}L}{h}. \quad (39)$$

Solving this equation with respect to the elliptic parameter $\tilde{m}(\alpha)$, we can obtain the energy and current

$$\begin{aligned} \mathcal{E}_1(\alpha) &= -\frac{2}{h} \left| \sqrt{1 - \frac{\tilde{m}}{1+2\cos^2(\alpha)} \cos(\alpha)} \right| \\ &+ \frac{\sqrt{2}}{h} [E(\tilde{m}) - E(\psi_0, \tilde{m})] - \frac{(2-m)L}{h^2} \end{aligned} \quad (40)$$

$$J_1(\alpha) = \frac{2}{h} \sqrt{1 - \frac{\tilde{m}}{1+2\cos^2(\alpha)}} \sin(\alpha) \operatorname{sign}[\cos(\alpha)] \quad (41)$$

The critical current at $\Phi = (k + 1/2)\Phi_0$ is given by $J_{\max,1} = \max_{\alpha}[J_1(\alpha)]$. At small L , $L/h \ll 1$, the maximum critical current is realized at the instability point of the rectangular lattice $\cos(\alpha) \approx L/h$ giving

$$J_{\max,1} \approx \frac{2}{h} \left(1 - \frac{L^2}{2h^2}\right). \quad (42)$$

It is always somewhat smaller than the ‘‘Fraunhofer’’ value $2/h$.

It was obtained in Section IV that the rectangular lattice is realized in ground state ($\alpha = 0$) at points $\Phi = (k + 1/2)\Phi_0$ for $L/h < l_1 = 0.675$. If, however, L/h is only slightly smaller than this value, the rectangular lattice becomes unstable with increasing current and the configuration at the critical current still corresponds to the deformed lattice. We found that there is another typical value of the ratio L/h , $L/h = l_2 \approx 0.484$, below which *the rectangular lattice remains stable up to the critical current*. Both typical values of h/L , $1/l_1$ and $1/l_2$, are marked in Fig. 6. One can see in that for both shown stack sizes, $L = 2.5$ and 4 , the rectangular lattice first appears around points $\Phi = (k + 1/2)\Phi_0$ when h/L exceeds $1/l_1$ and its stability range extends up to the critical current when h/L exceeds $1/l_2$.

For integer flux quanta, $\Phi = k\Phi_0$ ($hL = 2\pi k$), a changing-sign monotonic solution always realizes, $v_L = -v_0$. In the case $\cos \alpha > 0$ this corresponds to $\varphi_0 = \pi - \varphi_L = \arcsin[m(1 + 2\cos^2(\alpha))]^{-1/2}$ and Eq. (22) can be reduced to the form

$$\sqrt{m}(K(m) - F(\phi_0, m)) = \sqrt{2}L/h. \quad (43)$$

Solving this equation with respect to m , we can obtain the energy from Eq. (23) and current from Eq. (24)

$$\mathcal{E}_2 = -\frac{2}{h} \cos \phi_0 \cos \alpha + \frac{\sqrt{2}}{\sqrt{mh}} [E(m) - E(\phi_0, m)] - \frac{L}{mh^2} \quad (44)$$

$$J_2(\alpha) = \frac{2}{h} \cos \phi_0 \sin \alpha \quad (45)$$

The critical current at $\Phi = (k + 1/2)\Phi_0$ is given by $J_{\max,2} = \max_{\alpha}[J_2(\alpha)]$. At small L inequality $\cos \phi_0 \ll 1$ holds. In this limit, using relation $F(\phi_0, m) \approx K(m) - (\pi/2 - \phi_0)/\sqrt{1-m}$, we can approximately rewrite Eq. (43) as $\pi/2 - \phi_0 = (\sqrt{2L}/h)\sqrt{1-1/m}$. As $\sin \phi_0$ is close to one, Eq. (20a) gives $1/m \approx 1 + 2\cos^2(\alpha)$ and $\phi_0 = \pi/2 - (2L/h)\cos \alpha$. Therefore we obtain for the α -dependent current (45),

$$J_2(\alpha) \approx \frac{2L}{h^2} \sin 2\alpha. \quad (46)$$

The maximum is realized at $\alpha = \pi/4$ giving the following result for the critical current

$$J_{\max,2} \approx 2L/h^2, \quad (47)$$

i.e., it decays at large h as $1/h^2$ but never drops to zero as for usual Fraunhofer dependence. The behavior in the narrow-stack regime will be considered in more details in the next section. One can see that the critical currents at both maxima $J_{\max,\alpha}$ ($\alpha = 1, 2$) have the same scaling property: the product $hJ_{\max,\alpha}$ depends only on the ratio L/h . These scaling dependences are plotted in Fig. 5 in the plots for $L = 4$ and 6.

VI. NARROW-STACK REGIME

Lets consider in more detail the narrow-stack regime at $L/h \ll 1$. In this regime interaction with the boundaries is typically stronger than the bulk shearing interaction. As a consequence, the boundaries stabilize the rectangular lattice configuration in most part of the phase diagram. The exception is the narrow regions in the vicinity of the integer-flux-quanta points $\Phi = k\Phi_0$ where the interaction with the boundaries vanishes and the rectangular lattice loses its stability. The rectangular lattice also becomes unstable near the critical current. In this section we will study in details this behavior. Instead of using asymptotic behavior of elliptic integrals, it is more transparent to use as a starting point the equation for smooth alternating deformation (9), the boundary conditions (10) and the energy (12). It will be more convenient to use variable φ given by Eq. (16) (instead of v) from the very beginning, because it vanishes in the rectangular-lattice state. We also introduce a new variable for the lattice phase shift,

$$\beta \equiv \alpha + \pi/2 - hL/2,$$

which will facilitate a more compact presentation of results. In terms of the variables $\varphi(u)$ and β the energy (12) can be rewritten as

$$\begin{aligned} \mathcal{E}(\beta) \approx & -\frac{1}{h} \left[\cos \varphi_0 \sin \left(\beta + \frac{hL}{2} \right) - \cos \varphi_L \sin \left(\beta - \frac{hL}{2} \right) \right] \\ & + \int_0^L du \left[\frac{1}{8} \left(\frac{d\varphi}{du} \right)^2 - \frac{1 - \cos(2\varphi)}{2h^2} \right]. \end{aligned} \quad (48)$$

From this energy we obtain equation for $\varphi(u)$,

$$\frac{d^2\varphi}{du^2} + \frac{4}{h^2} \sin(2\varphi) = 0, \quad (49)$$

and the boundary conditions

$$\frac{d\varphi}{du}(0) = \frac{4}{h} \sin(\varphi_0) \sin \left(\beta + \frac{hL}{2} \right), \quad (50a)$$

$$\frac{d\varphi}{du}(L) = \frac{4}{h} \sin(\varphi_L) \sin \left(\beta - \frac{hL}{2} \right). \quad (50b)$$

For small L Eq. (49) can be solved as expansion with respect to powers of $u - L/2$,

$$\varphi = \varphi_a + a \left(u - \frac{L}{2} \right) - \frac{2(u - L/2)^2}{h^2} \sin(2\varphi_a) \quad (51)$$

with $\varphi_a = \varphi(L/2)$. Boundary conditions (50) give two equations for two unknown variables, the midpoint phase φ_a and the linear slope a . We obtain two types of solutions: (i) the rectangular-lattice solution $a = 0$, $\sin \varphi_a = 0$ and (ii) the deformed-lattice solution. In the leading order with respect to the small parameter L/h , the latter solution can be represented as

$$a \approx \frac{4}{h} \sin(\varphi_a) \sin \beta \cos(hL/2), \quad (52)$$

$$\cos(\varphi_a) \approx \frac{h}{L} \frac{\sin(hL/2) \cos \beta}{1 + 2 \sin^2 \beta \cos^2(hL/2)}. \quad (53)$$

As follows from the last equation, the deformed-lattice solution does not exist if

$$\frac{h}{L} \frac{|\sin(hL/2) \cos \beta|}{1 + 2 \sin^2 \beta \cos^2(hL/2)} > 1. \quad (54)$$

In this case the configuration must be the rectangular lattice. The solution (53) also includes the case of the ideal triangular lattice $\varphi_a = \pi/2$ which is always realized if either $\sin(hL/2) = 0$ or $\cos \beta = 0$. As we consider the region $L/h \ll 1$, both triangular and deformed lattices exist only in vicinity of these points.

For analysis of lattices, it is also useful to derive the energy as a function of the average lattice shift, β , and the relative phase shift between the neighboring layers, φ_a . For that we substitute expansion (51) up to the linear order with the phase gradient given by Eq. (52) into the energy (48) and obtain

$$\begin{aligned} \mathcal{E}(\varphi_a, \beta) \approx & -\frac{2}{h} \cos(\varphi_a) \sin \left(\frac{hL}{2} \right) \cos \beta \\ & - \frac{L}{h^2} \sin^2(\varphi_a) \left[1 + 2 \sin^2 \beta \cos^2 \left(\frac{hL}{2} \right) \right] \end{aligned} \quad (55)$$

In particular, the result (53) corresponds to the minimum of this energy with respect to φ_a when the condition (54) is satisfied. We will see that this relatively simple energy function of two variables, whose shape evolves with the

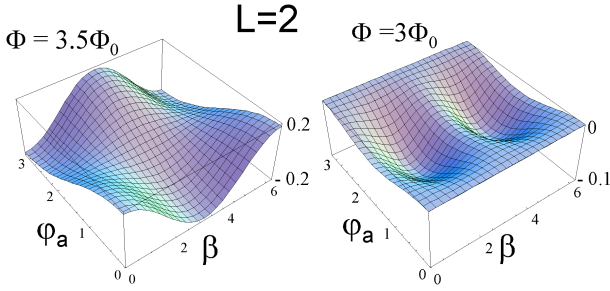


FIG. 7: Examples of the energy landscape (55) as a function of the average lattice shift β and the amplitude of the alternating phase deformation ϕ_a for $L = 2$ and $\Phi/\Phi_0 = 3.5$ and 3 . For $\Phi = 3.5\Phi_0$ the equivalent minima at $(\phi_a, \beta) = (0, \pi)$ and $(\pi, 0)$ correspond to the rectangular lattice, while for $\Phi = 3\Phi_0$ the minima at $(\phi_a, \beta) = (\pi/2, \pi/2)$ and $(\pi/2, 3\pi/2)$ correspond to the triangular lattice.

magnetic field, describes a surprisingly rich behavior in the vicinity of the integer-flux-quanta points. The typical energy landscapes for the cases of half-integer and integer flux quanta per junction are illustrated in Fig. 7.

Lets study zero-current ground states first. We start with stability analysis for the rectangular lattice which is realized at $\varphi_a = 0, \pi$ and gives ground state in the most part of phase space. In this case the energy is minimal with respect to β either at $\beta = 0$, for $\cos(\varphi_a)\sin(hL/2) > 0$, or at $\beta = \pi$, for $\cos(\varphi_a)\sin(hL/2) < 0$, see, e.g., left part of Fig. 7 where $\sin(hL/2) = -1$. Expanding the energy with respect to φ_a near the point $\varphi_a = 0$,

$$\mathcal{E}(\varphi_a, 0) \approx -\frac{2}{h} \left| \sin\left(\frac{hL}{2}\right) \right| + \frac{\varphi_a^2}{h} \left(\left| \sin\left(\frac{hL}{2}\right) \right| - \frac{L}{h} \right),$$

we conclude that the rectangular lattice is stable if

$$\left| \sin\left(\frac{hL}{2}\right) \right| > \frac{L}{h}, \quad (56)$$

which coincides with the condition (54) at $\beta = 0, \pi$. In real variables the condition (56) can be rewritten as

$$\frac{2\pi\Phi}{\Phi_0} \left| \sin\left(\frac{\pi\Phi}{\Phi_0}\right) \right| > \left(\frac{L}{\lambda_J}\right)^2. \quad (57)$$

Therefore even at small L/h the rectangular lattice is always unstable near the integer-flux-quanta points, $\Phi = k\Phi_0$. This is easy to understand: near these points the interaction with the boundaries vanishes and even small shearing interaction between the neighboring planar Josephson-vortex arrays becomes sufficient to induce instability with respect to the alternating deformations. Further analysis, however, will show that this instability takes place when the rectangular lattice does not give already the ground state, meaning that the system actually experiences a first-order transition.

For the deformed-lattice solution (53) the energy at fixed β is given by

$$\mathcal{E}(\beta) \approx -\frac{1}{L} \frac{\sin^2 \frac{hL}{2} \cos^2 \beta}{1 + 2 \sin^2 \beta \cos^2 \frac{hL}{2}} - \frac{L}{h^2} \left(1 + 2 \sin^2 \beta \cos^2 \frac{hL}{2} \right). \quad (58)$$

This energy always has extremums at $\beta = 0, \pi$, and $\pi/2$. As follows from Eq. (53), the state at $\beta = \pi/2$ always corresponds to the triangular lattice, $\varphi_a = \pi/2$. We find now the conditions that the energy reaches minima at these values of β . Consider first the point $\beta = 0$. Expanding the energy near this point,

$$\mathcal{E}(\beta) \approx -\frac{1}{L} \sin^2 \frac{hL}{2} - \frac{L}{h^2} + \frac{\beta^2}{L} \left[\sin^2 \frac{hL}{2} \left(1 + 2 \cos^2 \frac{hL}{2} \right) - \frac{2L^2}{h^2} \cos^2 \frac{hL}{2} \right],$$

we obtain that it corresponds to minimum if

$$\tan^2 \left(\frac{hL}{2} \right) \left[1 + 2 \cos^2 \left(\frac{hL}{2} \right) \right] > \frac{2L^2}{h^2}.$$

As $L/h \ll 1$, this inequality is valid almost everywhere except in the vicinity of the integer-flux-quanta points at which $\sin(hL/2) \rightarrow 0$ and $\cos^2(hL/2) \rightarrow 1$ where this condition can be rewritten in an approximate simpler form,

$$\left| \sin\left(\frac{hL}{2}\right) \right| > \frac{\sqrt{2}L}{\sqrt{3}h}.$$

Comparing this condition with the condition (56), we can see that the deformed lattice gives the energy minimum at $\beta = 0$ only within the narrow region given by

$$\sqrt{\frac{2}{3}} < \frac{h}{L} \left| \sin\left(\frac{hL}{2}\right) \right| < 1. \quad (59)$$

In this region the optimum value of φ_a for $\beta = 0$ is given by $\cos(\varphi_a) = (h/L) |\sin(hL/2)|$.

To find if the triangular lattice at the point $\beta = \pi/2$ gives the local energy minimum, we expand the energy (58) near this point, $\beta = \pi/2 - \zeta$,

$$\mathcal{E}(\beta) \approx -\frac{L}{h^2} \left(1 + 2 \cos^2 \frac{hL}{2} \right) + \zeta^2 \left(-\frac{1}{L} \frac{\sin^2 \frac{hL}{2}}{1 + 2 \cos^2 \frac{hL}{2}} + \frac{2L}{h^2} \cos^2 \frac{hL}{2} \right).$$

We can see that the value $\beta = \pi/2$ corresponds to energy minimum if

$$\frac{\tan^2 \frac{hL}{2}}{1 + 2 \cos^2 \frac{hL}{2}} < \frac{2L^2}{h^2}$$

or, approximately, $|\sin(hL/2)| < \sqrt{6}L/h$. We can conclude that near the integer-quanta points $\Phi = k\Phi_0$

($hL = 2k\pi$) the minimum location switches from $\beta = 0$ to $\beta = \pi/2$. In the intermediate region given approximately

$$\sqrt{\frac{2}{3}} < \frac{h}{L} \left| \sin\left(\frac{hL}{2}\right) \right| < \sqrt{6} \quad (60)$$

the energy has local minimums at both points, $\beta = 0$ and $\pi/2$. Moreover, in the region $(h/L) |\sin(hL/2)| > 1$ the minimum at $\beta = 0$ is realized by the rectangular lattice. This behavior indicates that *switching between the rectangular and triangular lattices in the ground state occurs via a first-order phase transition*.

To find the transition point, we compare the triangular-lattice energy,

$$\mathcal{E}_{\text{trian}} \equiv \mathcal{E}\left(\frac{\pi}{2}, \frac{\pi}{2}\right) = -\frac{L}{h^2} \left(1 + 2 \cos^2 \frac{hL}{2}\right),$$

with the rectangular-lattice energy,

$$\mathcal{E}_{\text{rect}} \equiv \mathcal{E}(0, 0) = -\frac{2}{h} \left| \sin\left(\frac{hL}{2}\right) \right|,$$

and obtain that the triangular lattice wins if

$$\left| \sin\left(\frac{hL}{2}\right) \right| < \frac{L}{2h} \left[1 + 2 \cos^2\left(\frac{hL}{2}\right)\right].$$

As this only happens near the points where $\cos^2(hL/2) \approx 1$, the equation for the transition points, h_t , can again be rewritten in a simpler form,

$$\left| \sin\left(\frac{h_t L}{2}\right) \right| = \frac{3}{2} \frac{L}{h_t}, \quad (61)$$

or in real units, in terms of flux per junction,

$$\frac{2\pi\Phi_t}{\Phi_0} \left| \sin\left(\frac{\pi\Phi_t}{\Phi_0}\right) \right| = \frac{3}{2} \left(\frac{L}{\lambda_J}\right)^2. \quad (62)$$

Comparing Eq. (61) with the stability criterion of the rectangular lattice (56), we indeed can see that before the rectangular lattice becomes unstable, it switches to the triangular lattice via a first-order phase transition. From this equation we can also obtain small shift of transition point with respect to the integer-flux-quantum point $\Phi = k\Phi_0$ as a function of the index k . Writing $\Phi_t = (k + f_{t,k})\Phi_0$, we compute

$$|f_{t,k}| \approx \frac{3}{4\pi^2 k} \left(\frac{L}{\lambda_J}\right)^2 \ll 1. \quad (63)$$

The discussed behavior is illustrated in Fig. 8 in which the β -dependences of the energy and current are plotted for $L = 2$ and several values of Φ above the point $3\Phi_0$. The contour plot of energy at the transition point is also shown.

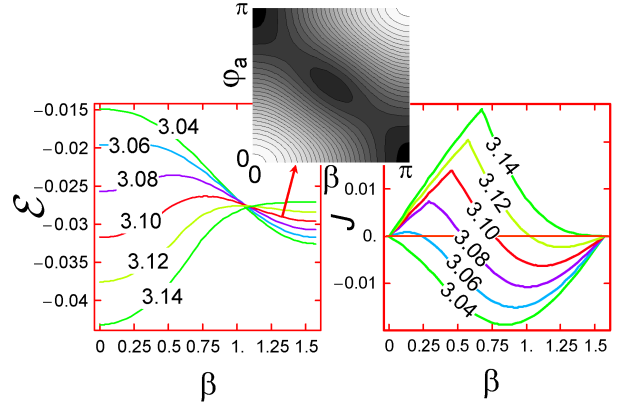


FIG. 8: The dependences of the energy (left) and current (right) on the lattice phase shift β for $L = 2\lambda_J$ slightly above the point $\Phi = 3\Phi_0$ (curves are marked by the values of Φ/Φ_0). One can observe several features discussed in details in the text. Close the $\Phi = 3\Phi_0$ for $\Phi < 3.1\Phi_0$ the global energy has minimum at $\beta = \pi/2$ corresponding to the triangular lattice (Eq. (63) actually gives $\Phi_t = (3 + 1/\pi^2)\Phi_0$ for the transition point). Above this point the global minimum is given by the rectangular lattice at $\beta = 0$. Within narrow range of Φ the energy has minima at both $\beta = 0$ and $\pi/2$. The rectangular lattice appears at the local minimum at $\beta = 0$ for $\Phi \geq 3.08\Phi_0$ but it becomes unstable with increasing β . The instability points are seen as kinks in the $J(\beta)$ curves. In some range of Φ the absolute value of current has two local maxima within $0 < \beta < \pi/2$. The critical current switches between these maxima with increasing Φ . Inset shows the contour plot of energy near the transition point, at $\Phi = 3.1\Phi_0$.

Let us investigate now current-carrying states and behavior of the critical current. In the region given by Eq. (54) the current in the rectangular-lattice state is

$$J(\beta) = \frac{2}{h} \left| \sin\left(\frac{hL}{2}\right) \right| \sin \beta, \quad (64)$$

where we assumed for definiteness that $\cos \varphi_a \sin(hL/2) > 0$. If the condition (54) is violated then the deformed lattice is realized. In this case, differentiating the energy (58) with respect to β , we obtain the current in the deformed-lattice state (including the triangular lattice)

$$J(\beta) = \left(\frac{\sin^2 \frac{hL}{2} (1 + 2 \cos^2 \frac{hL}{2})}{L (1 + 2 \sin^2 \beta \cos^2 \frac{hL}{2})^2} - \frac{2L \cos^2 \frac{hL}{2}}{h^2} \right) \sin 2\beta, \quad (65)$$

$$\text{for } \frac{h}{L} \frac{|\sin \frac{hL}{2} \cos \beta|}{1 + 2 \sin^2 \beta \cos^2 \frac{hL}{2}} < 1.$$

In particular, at $hL = 2\pi k$ this formula reproduces results (46) and (47) obtained from the elliptic-integral representation.

Consider first the region where the ground state is given by the rectangular lattice. Maximum current in

this state would be achieved at $\beta = \pi/2$ but the condition (54) always breaks down before that. From this condition we compute the value of β at which the rectangular lattice becomes unstable

$$|\cos \beta_t| = \frac{2 \frac{L}{h} (1 + 2 \cos^2 \frac{hL}{2})}{\left| \sin \frac{hL}{2} \right| + \sqrt{\sin^2 \frac{hL}{2} + \frac{8L^2}{h^2} \cos^2 \frac{hL}{2} (1 + 2 \cos^2 \frac{hL}{2})}}. \quad (66)$$

In a wide range of parameters, away from the regions given by Eq. (61), the maximum current is achieved at this instability point

$$J_c = \frac{2}{h} \left| \sin \left(\frac{hL}{2} \right) \right| \sin \beta_t. \quad (67)$$

In particular, in most part of the parameter space, for $|\tan(hL/2)| \gg L/h$ we obtain much simpler results

$$|\cos \beta_t| \approx \frac{L}{h} \frac{1 + 2 \cos^2 \frac{hL}{2}}{\left| \sin \frac{hL}{2} \right|}, \quad (68)$$

$$J_c \approx \frac{2}{h} \left| \sin \left(\frac{hL}{2} \right) \right| \left[1 - \left(\frac{L}{h} \right)^2 \frac{(1 + 2 \cos^2 \frac{hL}{2})^2}{2 \sin^2 \frac{hL}{2}} \right]. \quad (69)$$

In this region the critical current is only slightly smaller than the ‘‘Fraunhofer’’ result $(2/h) |\sin(hL/2)|$. At the half-integer-flux-quanta points $hL = (2k + 1)\pi$ these equations reproduce result (42) obtained from the elliptic-integrals representation. The property that the rectangular lattice is always unstable at some lattice displacement β also has important dynamic consequences. It means that the lattice can not maintain its static rectangular configuration when it starts to move.

The critical current has a nontrivial behavior in the vicinity of points $hL = 2\pi k$ where $|\sin(\frac{hL}{2})| \ll 1$ and general formula (65) can be simplified as

$$J(\beta) \approx \frac{2L}{h^2} \left(1 - \frac{3h^2 \sin^2(\frac{hL}{2})}{2L^2 (2 - \cos 2\beta)^2} \right) \sin 2\beta.$$

This gives the critical current near $hL = 2\pi k$

$$J_c(h, L) \approx \frac{2L}{h^2} \left(1 - \frac{3h^2 \sin^2(\frac{hL}{2})}{2L^2} \right),$$

for $\sin(hL/2) \ll L/h$. This results shows that *the dependence $J_c(\Phi)$ for junction stacks always has local maxima at $\Phi = k\Phi_0$* , in contrast to the Fraunhofer dependence for which the critical current vanishes at these points. To find the critical current behavior in the whole field range in the region $h/L \gg 1$, we numerically found maximum of $J(\beta)$ with respect to β and different $hL = 2\pi\Phi/\Phi_0$ and L . Figure 9 illustrates the field dependence of critical current and current dependence of the lattice structure within one oscillation period $2.5\Phi_0 < \Phi < 3.5\Phi_0$ for $L = 2\lambda_J$. To visualize the lattice structures, we represent

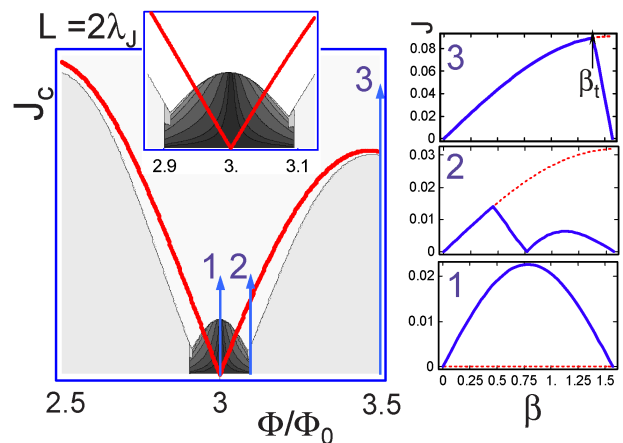


FIG. 9: The main plot: the field dependence of the critical current for $L = 2\lambda_J$ within one oscillation period $2.5\Phi_0 < \Phi < 3.5\Phi_0$. The grey level codes the value of $|\cos \varphi_a|$ with the light grey color in most part of the plot corresponding to the rectangular lattice $|\cos \varphi_a| = 1$ and the black color near $\Phi/\Phi_0 = 3$ corresponding to triangular lattice $|\cos \varphi_a| = 0$. The solid line shows the Fraunhofer dependence $\sin(\pi\Phi/\Phi_0)/(\pi\Phi/\Phi_0)$. The inset above shows blowup of the region near $\Phi/\Phi_0 = 3$. Plots at the right side illustrate representative dependences $|J(\beta)|$ for three values of Φ marked by arrows. Dashed curves in these plots show corresponding dependences for usual small junction. The kinks in the $J_c(\Phi)$ curve at $\Phi/\Phi_0 \approx 3 \pm 0.085$ occur due to the switching between different maxima in the $|J(\beta)|$ dependence.

the values of $|\cos \varphi_a|$ by grey level. In most part of the current-field diagram the rectangular lattice is realized shown by light grey ($|\cos \varphi_a| = 1$). The triangular lattice shown by black ($|\cos \varphi_a| = 0$) appears in the ground state only in vicinity of the point $\Phi = 3\Phi_0$. Exactly at this point the lattice remains triangular up to the critical current. Slightly away from this point the lattice deforms with increasing current. In the range of parameters given by Eq. (60) the dependence $|J(\beta)|$ has two maxima within $0 < \beta < \pi/2$ (see left plot in Fig. 8). As a consequence, the field dependence of the critical current has kinks related to switching between these maxima.

VII. SLOW DYNAMICS IN OVERDAMPED REGIME: OSCILLATIONS OF THE FLUX-FLOW VOLTAGE

When the external current flowing across the layers exceeds the critical current, the lattice starts to move. In general, dynamic behavior is quite complicated. A simple situation is realized only at slow lattice motion in the overdamped case when the lattice deformations have time to adjust to the current lattice position. In this case the lattice moves in the periodic potential given by its static energy (12) and one can use static results to predict the I-V dependences. On the other hand, one

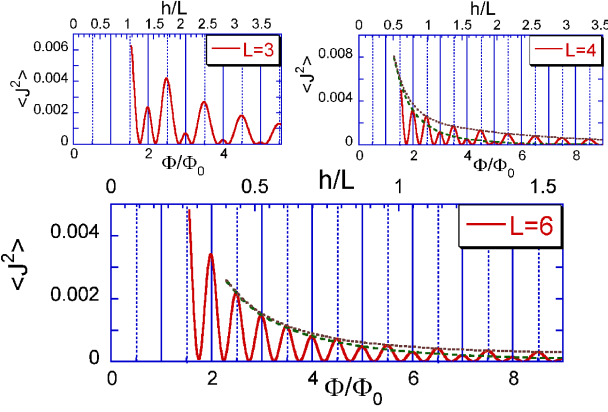


FIG. 10: The representative field dependences of mean-squared average of current, $\langle J^2(\alpha) \rangle$, with respect to the lattice displacements which determines the amplitude of relative voltage oscillations $\delta U/U_{ff}$ at slow velocities via Eq. (72).

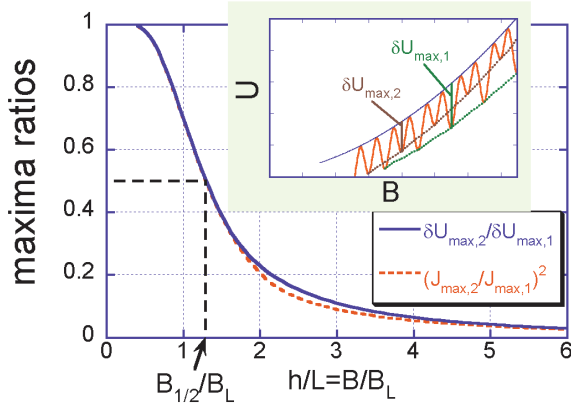


FIG. 11: The field dependence of the ratio of voltage-oscillation maxima at integer-flux-quanta points ($\delta U_{max,2}$) and at half-integer-flux-quanta points ($\delta U_{max,1}$). The inset illustrates definitions of $\delta U_{max,1}$ and $\delta U_{max,2}$ in the schematic voltage-field dependence. For comparison we also show plot of the ratio of the critical-current maxima squared $(J_{max,2}/J_{max,1})^2$. Extraction of the typical field $B_{1/2}$ from the analysis of the voltage oscillations allows accurately evaluate the anisotropy factor γ using Eq. (73).

can expect that the voltage oscillations are less sensitive to inhomogeneities than the critical-current oscillations, because the homogeneously moving lattice smears away disorder. The critical current is also smeared by thermal fluctuations. These are possible reasons why it is easier to observe and interpret the magnetic oscillations in the flux-flow resistivity than in the critical current.^{8,15,16,17}

In general, the dynamic behavior also depends on the dissipation mechanism. In BSCCO in a wide range of magnetic fields the flux-flow resistivity is mainly determined by the in-plane quasiparticle conductivity σ_{ab} .²⁵

Only when the magnetic field exceeds a typical value $B_\sigma = \sqrt{\sigma_{ab}/\sigma_c} \Phi_0 / (\sqrt{2} \pi \gamma^2 s^2)$, the c-axis conductivity, σ_c , gives dominating contribution to the flux-flow dissipation. In this limit the flux-flow resistivity becomes field-independent. In BSCCO the field B_σ is typically several times larger than the crossover field B_{cr} . An important feature of the in-plane dissipation regime at $B < B_\sigma$ is that the lattice velocity at fixed applied current is very sensitive to lattice structure, the smallest velocity is realized for the triangular lattice and the largest velocity is realized for the rectangular lattice. As the lattice structure in the regime $B \gtrsim B_L$ continuously changes with lattice displacement, the dynamic behavior in this regime is rather complicated. To avoid this complications, we limit ourself here by a simple case of dominating c-axis dissipation in the crossover region, $B_L > B_\sigma$. In this case the viscous-friction coefficient weakly depends on lattice structure.

In the case of structure-independent viscous-friction coefficient ν_{ff} , time variation of the lattice phase shift obeys equation

$$\nu_{ff} \frac{d\alpha}{dt} + J(\alpha) = J_{\text{ext}}, \quad (70)$$

where J_{ext} is the external current, the current $J(\alpha) \equiv J(\alpha, hL, h)$ is given by Eq. (13) (for brevity we again skip in equations its dependence on the magnetic field and size), and the viscosity coefficient, ν_{ff} , is related to the flux-flow resistance of the stack, R_{ff} ,

$$\nu_{ff} = \frac{N \Phi_0}{2\pi c R_{ff}}.$$

where N is the number of junctions in the stack. The voltage drop per one junction U is related to $d\alpha/dt$ by the Josephson relation

$$U = \frac{\Phi_0}{2\pi c} \frac{d\alpha}{dt}.$$

Solution of Eq. (70) is given by the implicit relation

$$\int_0^\alpha \frac{\nu_{ff} d\alpha'}{J_{\text{ext}} - J(\alpha')} = t,$$

from which we obtain the average phase change rate,

$$\overline{\frac{d\alpha}{dt}} = \left[\frac{1}{\pi} \int_0^\pi \frac{\nu_{ff} d\alpha}{J_{\text{ext}} - J(\alpha)} \right]^{-1},$$

and the flux-flow voltage

$$\frac{U}{U_{ff}} = \left[\frac{J_{\text{ext}}}{\pi} \int_0^\pi \frac{d\alpha}{J_{\text{ext}} - J(\alpha)} \right]^{-1} \quad (71)$$

with $U_{ff} = R_{ff} J$ being the bare flux-flow voltage without the periodic potential. As the current $J(\alpha) \equiv J(\alpha, hL, h)$ oscillates with the magnetic field, this flux-flow voltage will also experience similar field oscillations. In particular, when the external current significantly exceeds the critical current, $J_{\text{ext}} \gg J_c$, we obtain weak oscillating correction to the flux-flow voltage,

$$\delta U = U - U_{ff},$$

$$\delta U/U_{ff} \approx -\langle J^2(\alpha) \rangle / J_{\text{ext}}^2, \quad (72)$$

where $\langle f(\alpha) \rangle \equiv (1/\pi) \int_0^\pi f(\alpha) d\alpha$ is the average with respect to the lattice phase shift. As $\delta U \propto \langle J^2(\alpha) \rangle$, the behavior of δU is overall similar to the behavior of the critical current but the amplitude of voltage oscillations roughly scales as the critical current squared. Figure 10 shows the field dependences of the average $\langle J^2(\alpha) \rangle$, which determines the amplitude of weak voltage oscillations, for three junctions sizes, $L = 3, 4$, and 6 .

Consider in more details behavior of δU at the points $\Phi = (j/2)\Phi_0$. To find the amplitude of the small voltage correction, $\delta U_{max,1}$, at the half-integer flux quanta points, $\Phi = (k+1/2)\Phi_0$, we have to find the α -average of $J_1^2(\alpha)$ where the current $J_1(\alpha)$ is given by Eq. (41) with the parameter \tilde{m} given by Eq. (39). Similarly, the amplitude of the voltage oscillation at the points $\Phi = k\Phi_0$, which we notate as $\delta U_{max,2}$, is determined by $\langle J_2^2(\alpha) \rangle$ where the current $J_2(\alpha)$ is given by Eq. (45) with the parameter m given by Eq. (43). Figure 11 shows the computed field dependence of the ratio $\delta U_{max,2}/\delta U_{max,1}$ together with the ratio $(J_{max,2}/J_{max,1})^2$. In practice, to extract the ratio $\delta U_{max,2}/\delta U_{max,1}$ from experimental voltage-field dependence, one should plot smooth curves via local maxima and two sets of local minima as it is illustrated in the inset of Fig. 11, subtract the two minima curves from the maxima curve, and compute the ratio of the differences. One can see that the field dependences of $\delta U_{max,2}/\delta U_{max,1}$ and $(J_{max,2}/J_{max,1})^2$ are almost identical. This plot gives possibility for accurate determination of the anisotropy factor from the voltage oscillations using the field scale. In particular, the ratio $\delta U_2/\delta U_1$ drops to 0.5 at the field $B_{1/2} = 1.302B_L = 1.302\Phi_0 L/(2\pi\gamma^2 s^3)$ (see Fig. 11) meaning that γ can be extracted from this field as

$$\gamma \approx 330 \sqrt{\frac{L[\mu m]}{B_{1/2}[T]}}. \quad (73)$$

where we used the BSCCO interlayer spacing $s \approx 1.56$ nm. For example, using data reported in Ref. 15 for the sample H55 with $L = 5.5 \mu m$, we estimate $B_{1/2} \approx 3.6$ T giving a very reasonable estimate $\gamma \approx 408$. This estimate is significantly larger than the value $\gamma \approx 110$ obtained by the authors themselves and the difference comes from the value of the numerical constant in the crossover field.

We have to mention that an alternative mechanism of $\Phi_0/2$ -periodic voltage oscillations at fixed current exists at high lattice velocities due to switching between the Fiske steps.²⁶ However, experimentally, the most regular voltage oscillations are observed at voltages much smaller than the first Fiske voltage.^{8,15,16,17}

VIII. SUMMARY

In summary, we studied magnetic oscillations of the critical current and lattice configurations in stacks of in-

trinsic Josephson junctions, which are realized in mesas fabricated from layered high-temperature superconductors. Depending on the stack lateral size, oscillations may have either the period of half flux quantum per junction (wide-stack regime) or one flux quantum per junction (narrow-stack regime). We studied in detail the crossover between these two regimes. Typical size separating the regimes is proportional to the magnetic field meaning that the crossover can be driven by the magnetic field. In the narrow-stack regime the lattice structure experiences periodic series of first-order phase transitions between aligned rectangular configuration and triangular configuration. The triangular configurations in this regime is realized only in narrow regions near magnetic-field values corresponding to integer number of flux quanta per junction. For slow lattice motion similar crossover can also be observed in the oscillations of the flux-flow resistivity. Quantitative study of the crossover allows for a very accurate evaluation of the anisotropy factor.

IX. ACKNOWLEDGEMENTS

The author thanks I. Kakeya, Y. Latyshev, and T. Hatano for useful discussions of experimental data and to L. Bulaevskii for numerous discussion of related theoretical issues. This work was supported by the U. S. DOE, Office of Science, under contract # DE-AC02-06CH11357.

APPENDIX A: REGIONS OF MONOTONIC SAME-SIGN SOLUTIONS FOR $v(u)$

One can distinguish two types of monotonic solutions depending on whether or not the smooth phase $v(u) = (\varphi(u) - \pi/2)/2$ changes sign inside the junction (see Fig. 2). For the changing-sign solution the condition $0 < m < 1$ always holds. In this Appendix we find the boundary values of α separating these two types of monotonic solutions. For definiteness, we consider the region $2k\pi < hL < (2k+1)\pi$ and $-\pi/2 + hL - 2k\pi < \alpha < \pi/2$ (grey area in the lower part of the phase diagram in Fig. 2). For the monotonic changing-sign solution in this range we have $0 < \varphi_0 < \pi/2$, $\pi/2 < \phi_L < \pi$, i.e.,

$$\varphi_0 = \arcsin \sqrt{\frac{1/m}{1 + 2 \cos^2(\alpha)}},$$

$$\varphi_L = \pi - \arcsin \sqrt{\frac{1/m}{1 + 2 \cos^2(hL - \alpha)}}.$$

There are two boundaries in the region, one corresponding to the condition $\phi_0 = \pi/2$ ($v_0 = 0$) below $\alpha = \pi/2$ and another corresponding to $\phi_L = \pi/2$ ($v_L = 0$) above $\alpha = -\pi/2 + hL - 2k\pi$ (see Fig. 2). For the first boundary,

$\alpha_0(h, L)$, from Eqs. (20a) and (22) we obtain

$$\sqrt{m_0} \left[K(m_0) - F \left(\arcsin \sqrt{\frac{1/m_0}{1+2\cos^2(hL-\alpha_0)}}, m_0 \right) \right] = \frac{\sqrt{8}L}{h}, \quad (\text{A1a})$$

$$m_0 = \frac{1}{1+2\cos^2(\alpha_0)}, \quad (\text{A1b})$$

where $K(m) = F(\pi/2, m)$ is the complete elliptic integral of the first kind²⁴ and we used the identity $F(\pi - \beta, m) - K(m) = K(m) - F(\beta, m)$. Analyzing similar equation for the second boundary, $\alpha_L(h, L)$, we find that it is related to $\alpha_0(h, L)$ as $\alpha_L(h, L) = hL - 2k\pi - \alpha_0(h, L)$. One can check that $\alpha_0(h, L) \rightarrow \pi/2$ for $hL \rightarrow 2k\pi, (2k+1)\pi$ and for $L \rightarrow \infty$, i.e., the region of the same-sign monotonic solution vanish in these limits.

APPENDIX B: WEAK FINITE-SIZE EFFECTS AT LARGE L

In this Appendix we derive finite-size corrections to the critical current due to interaction between the surface solitons. Consider for definiteness the case of monotonic solution. The nonmonotonic solution can be treated similarly. In the limit $L/h \gg 1$ the parameter m in Eq. (21) is close to one. Separating small correction, $m = 1 - \eta/2$ with $\eta \ll 1$, we evaluate the integral as

$$\int_{v_0}^{v_L} \frac{dv}{\sqrt{1+\eta/2-\cos^2(2v)}} \approx \frac{1}{2} \ln \left(-\frac{32}{\eta} \tan v_0 \tan v_L \right).$$

This gives the following result for η

$$\eta \approx -32 \tan v_0 \tan v_L \exp \left(-\sqrt{8}L/h \right), \quad (\text{B1})$$

corresponding to the elliptic-function parameter $m \approx 1 + 16 \tan v_0 \tan v_L \exp \left(-\sqrt{8}L/h \right)$. The boundary conditions can be represented as

$$\cos(2v_0) \approx \frac{1+\eta/4}{\sqrt{1+2\cos^2(\alpha)}},$$

$$\cos(2v_L) \approx \frac{1+\eta/4}{\sqrt{1+2\cos^2(hL-\alpha)}}.$$

One can neglect shift of η due to the finite-size corrections to v_0 and v_L . Without interaction between edge deformations, the energy can be written as¹²

$$\mathcal{E}_0 = \frac{1}{h} \sin(2v_{00}) \cos(\alpha) - \frac{1}{h} \sin(2v_{L0}) \cos(hL - \alpha) + \frac{1}{h} \int_{v_{00}}^{v_{L0}} dv \sqrt{1 - \cos(4v)} - L \frac{2}{2h^2} = \frac{1}{h\sqrt{2}} \left(2 - \sqrt{2 + \cos 2\alpha} - \sqrt{2 + \cos 2(\alpha - hL)} \right) - \frac{L}{h^2}.$$

where v_{00} and v_{L0} are the surface deformations neglecting finite-size correction,

$$\tan v_{00} = \frac{1 - \sqrt{1 + 2\cos^2 \alpha}}{\sqrt{2} \cos \alpha},$$

$$\tan v_{L0} = -\frac{1 - \sqrt{1 + 2\cos^2(\alpha - hL)}}{\sqrt{2} \cos(\alpha - hL)}.$$

The finite-size correction to the energy change can now be estimated as

$$\delta\mathcal{E} = \frac{1}{h} \int_{v_{00}}^{v_{L0}} dv \left(\sqrt{1+\eta-\cos(4v)} - \sqrt{1-\cos(4v)} \right) - \frac{L\eta}{2h^2} \approx \frac{\eta}{h\sqrt{32}}.$$

Therefore, the total total energy can be written as

$$\mathcal{E}(\alpha, h, hL) = -\frac{L}{h^2} + \frac{1}{\sqrt{2}h} \left(2 - \sqrt{2 + \cos(2\alpha)} - \sqrt{2 + \cos[2(\alpha - hL)]} \right) + \frac{8\sqrt{2}}{h} \frac{\cos(\alpha) \cos(\alpha - hL) \exp(-\sqrt{8}L/h)}{\left(1 + \sqrt{2 + \cos(2\alpha)} \right) \left(1 + \sqrt{2 + \cos[2(\alpha - hL)]} \right)}. \quad (\text{B2})$$

The last correction term describes the exponentially small interaction energy between the surface solitons. It is important to note that the finite-size correction breaks π -periodicity with respect to parameter hL meaning that the states with $\Phi = k\Phi_0$ and $\Phi = (k + 1/2)\Phi_0$ are not equivalent any more.

For the Josephson current we obtain

$$J(\alpha, h, hL) = \frac{1}{\sqrt{2}h} \left(\frac{\sin 2\alpha}{\sqrt{2 + \cos 2\alpha}} + \frac{\sin 2(\alpha - hL)}{\sqrt{2 + \cos 2(\alpha - hL)}} \right) + \frac{8\sqrt{2}}{h} \exp \left(-\frac{\sqrt{8}L}{h} \right) \frac{\partial}{\partial \alpha} \left[\frac{\cos \alpha \cos(\alpha - hL)}{\left(1 + \sqrt{2 + \cos 2\alpha} \right) \left(1 + \sqrt{2 + \cos 2(\alpha - hL)} \right)} \right].$$

Assuming that without the finite-size correction the maximum current flows at $\alpha = \alpha_m(hL)$, we obtain for the

finite-size correction to the critical current

$$\delta J_c(h, hL) = \frac{8\sqrt{2}}{h} \exp\left(-\frac{\sqrt{8}L}{h}\right) \frac{\partial}{\partial \alpha} \left[\frac{\cos \alpha \cos(\alpha - hL)}{\left(1 + \sqrt{2 + \cos(2\alpha)}\right) \left(1 + \sqrt{2 + \cos[2(\alpha - hL)]}\right)} \right]_{\alpha=\alpha_m(hL)}$$

In particular, near the maxima $hL = \pi j$ ($\Phi = j\Phi_0/2$), using the result¹² $\alpha_m(0) = 0.921$, we obtain result (37).

-
- ¹ R. Kleiner and P. Müller, Phys. Rev. B **49**, 1327 (1994).
² A. A. Yurgens, Supercond. Sci. Technol. **13**, R85 (2000).
³ L. N. Bulaevskii and J. R. Clem, Phys. Rev. B, **44**, 10234 (1991).
⁴ L. N. Bulaevskii, M. Zamora, D. Baeriswyl, H. Beck, and J. R. Clem, Phys. Rev. B, **50**, 12831 (1994); R. Kleiner, P. Müller, H. Kohlstedt, N. F. Pedersen, and S. Sakai, Phys. Rev. B, **50**, 3942 (1994).
⁵ J. U. Lee, J. E. Nordman, and G. Hohenwarter, Appl. Phys. Lett., **67**, 1471 (1995); J. U. Lee, P. Guptasarma, D. Hornbaker, A. El-Kortas, D. Hinks, and K. E. Gray Appl. Phys. Lett., **71**, 1412 (1997).
⁶ G. Hechtfisher, R. Kleiner, A. V. Ustinov, and P. Müller, Phys. Rev. Lett. **79**, 1365 (1997); G. Hechtfisher, R. Kleiner, K. Schlenga, W. Walkenhorst, P. Müller, and H. L. Johnson, Phys. Rev. B, **55**, 14638 (1997).
⁷ Yu. I. Latyshev, P. Monceau, and V. N. Pavlenko, Physica C **282-287**, 387 (1997); Physica C **293**, 174 (1997); Yu. I. Latyshev, M. B. Gaifullin, T. Yamashita, M. Machida, and Y. Matsuda, Phys. Rev. Lett., **87**, 247007 (2001).
⁸ S. Ooi, T. Mochiku, and K. Hirata, Phys. Rev. Lett. **89**, 247002 (2002).
⁹ J. M. Rowel, Phys. Rev. Lett. **11**, 200 (1963).
¹⁰ L. N. Bulaevskii, J. R. Clem, and L. I. Glazman, Phys. Rev. B, **46**, 350 (1992).
¹¹ C. S. Owen and D. J. Scalapino, Phys. Rev., **164**, 538 (1967); S. Pagano, B. Ruggiero, and E. Sarnelli, Phys. Rev. B **43** 5364-5369 (1991); J. G. Caputo, N. Flytzanis, Y. Gaididei, N. Stefanakis, and E. Vavalis, Supercond. Sci. Tech. **13**, (423) 2000; P. R. Auvil, J. B. Ketterson, and S. R. Maglic, J. Low Temp. Phys. **115**, 45, (1999).
¹² A. E. Koshelev, Phys. Rev. B **66**, 224514 (2002).
¹³ Note that in the previous paper¹² the typical length scale l_B has been defined with different numerical factor, $l_B = L_B/2\sqrt{2}$. This earlier definition was based on the decay length of the surface deformation. A more detailed study of this paper shows that the crossover between the stack regimes is better described by the condition $L \sim L_B$.
¹⁴ M. Machida, Phys. Rev. Lett. **90**, 037001 (2003).
¹⁵ I. Kakeya, M. Iwase, T. Yamazaki, T. Yamamoto, K. Kadowaki, *Proceedings of FIMS/ITS-NS/CTC/PLASMA 2004, Tsukuba, 24-28, November, 2004*, cond-mat/0503498.
¹⁶ B. Y. Zhu, H. B. Wang, S. M. Kim, S. Urayama, T. Hatano, and X. Hu, Phys. Rev. B **72**, 174514 (2005).
¹⁷ S. Urayama, T. Hatano, H. B. Wang, M. Nagao, S. M. Kim, J. Arai, cond-mat/0602659.
¹⁸ Yu. I. Latyshev, V. N. Pavlenko, A. P. Orlov, and X. Hu, Pis'ma ZhETF, **82**, 251 (2005) (JETP Letters, **82**, 232 (2005)).
¹⁹ M. Nagao, S. Urayama, S. M. Kim, H. B. Wang, K. S. Yun, Y. Takano, T. Hatano, I. Iguchi, T. Yamashita, M. Tachiki, H. Maeda, and M. Sato, Phys. Rev. B **74**, 054502 (2006).
²⁰ In a complete soliton the phase changes from 0 to $\pm 2\pi$. In the partial (surface) soliton the phase changes from some value ϕ_s at the surface to 0 far away from the surface.
²¹ A. Irie and G. Oya, Supercond. Sci. Technol. **20**, S18 (2007).
²² A. E. Koshelev, Physica C, **437 - 438**, 157 (2006).
²³ M. Machida, Phys. Rev. Lett. **96**, 097002 (2006).
²⁴ M. Abramovitz and I. A. Stegun, *Handbook of Mathematical Functions*, Nat. Bureau of Standards, 1964.
²⁵ A. E. Koshelev, Phys. Rev. B **62**, R3616 (2000); Yu. I. Latyshev, A. E. Koshelev, and L. N. Bulaevskii, Phys. Rev. B **68**, 134504 (2003).
²⁶ A. V. Ustinov and N. F. Pedersen, Phys. Rev. B **72**, 052502 (2005).